

Laboratory Quantification of Geomechanical Properties of Hydrate-Bearing Sediments in the Shenhu Area of the South China Sea at In-Situ Conditions

Liang Jinqiang¹, Wei Jiangong¹, Nikolaus Bigalke^{2*}, John Roberts², Peter Schultheiss², Melanie Holland²

¹*Guangzhou Marine Geological Survey, Guangzhou, Guangdong, 510075, China;*

²*GEOTEK Ltd, 4 Sopwith Way, Daventry, Northamptonshire, NN11 8PB, United Kingdom*

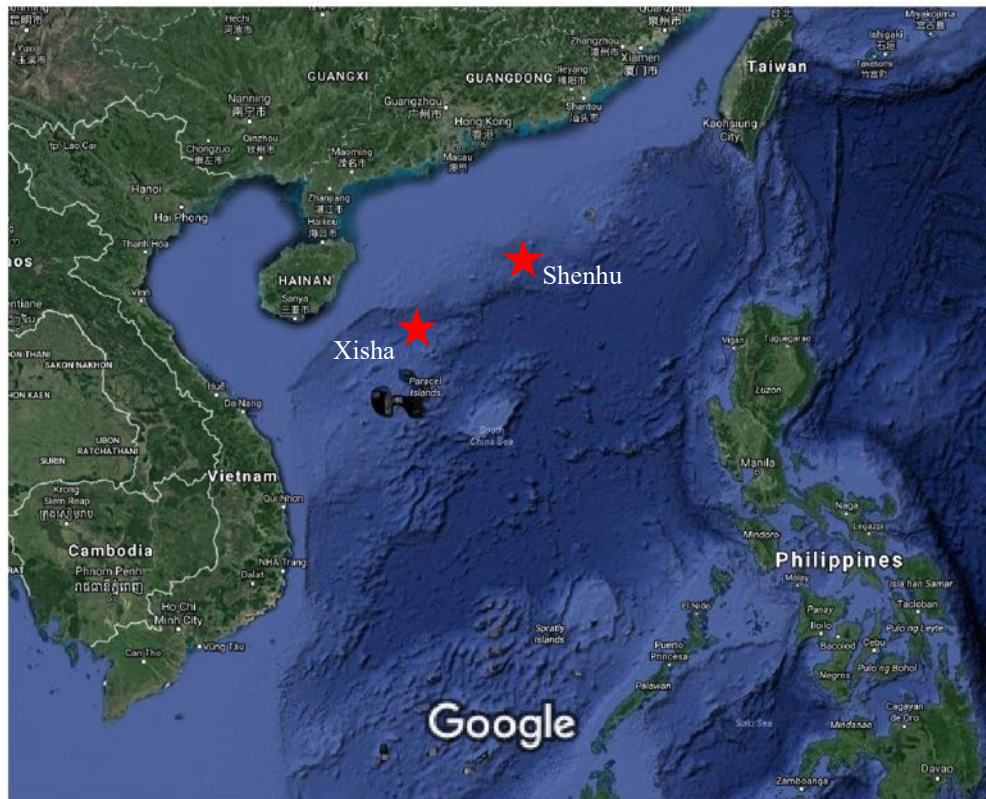
*Corresponding author: nikolaus.bigalke@geotek.co.uk

Abstract

We report on the characterisation of hydrate-bearing sediment cores from the South China Sea in terms of elastic properties, permeability, shear strength and gas hydrate saturation. The measurements were performed with Geotek's PCATS Triaxial testing apparatus during expedition GMGS 4, Leg 3 from June – August 2016. The geomechanical effects arising from the unique nature of the hydrate bearing sediments were studied under in-situ conditions in a total of 10 samples. The suite of analyses was complemented by measurements of P-wave velocity, gamma density and grain size. With the exception of permeability, the tested parameters showed a good correlation to gas hydrate saturation.

Motivation

Production of gas via purposeful destabilisation of natural gas hydrates in-situ changes the soil parameters in the host sediment. This may complicate the production process, for example via mobilisation of host sediment and loss of well-log stability due to the removal of the hydrate cement and to the reduction of the effective stress caused by free gas release. In offshore scenarios loss of sediment strength concomitant to gas hydrate destabilisation entails the added risk of submarine slope failures with potentially catastrophic effects. Due to the immense cost of field trials, efficiency and safety of gas production from hydrates is predominantly evaluated via numerical modelling [1]. Thanks to past advances in remote sensing techniques and to a good availability of conventional soil samples, underlying reservoir parameters are well constrained in terms of geophysics and geochemistry. However, the geomechanics of hydrate reservoirs remain poorly understood. The gold standard to obtain these data is the analysis of representative sediment samples in geomechanical testing apparatuses, ideally at in-situ stress conditions. Sediment samples containing gas hydrates complicate the testing as P -/ T -coordinates must remain within the hydrate stability field during sampling, recovery as well as throughout testing. Apart from pressure coring tools, allowing the recovery of undisturbed hydrate-bearing sediment cores, innovative core processing and analytical techniques have been developed that enable subsampling, transfer and analysis of pristine hydrate-bearing sediment cores at in situ hydrostatic pressure [2,3,4,5]. To further mimic seabed conditions by re-application of the in-situ effective stress in addition to hydrostatic pressure, the PCATS Triaxial testing apparatus has been developed [6]. Installed in a seagoing container, PCATS Triaxial has most recently been deployed during the Chinese Guangzhou Marine Geological Survey 4 (GMGS 4) expedition to the South China Sea. The expedition was performed on R/V Fugro Voyager from May – August 2016 and targeted the Shenhu area, previously visited during GMGS 1, GMGS 2 and GMGS 3 as well as the Xisha area, which was visited for the first time during GMGS 4. The previous expeditions revealed rich, clayey-silt-hosted gas hydrate occurrences in the Shenhu area. The aim of GMGS 4 was to complement findings on previously visited gas hydrate deposits and explore new sites in both Shenhu and Xisha areas. Within this scheme PCATS Triaxial was used to provide in situ sediment permeabilities, shear strengths and elastic properties (small strain shear strength, S-wave velocities) from intact, pressured core subsamples. These data were evaluated against gas hydrate saturations, which were determined via controlled degassing at the end of each geomechanical test program.



Imagery ©2016 TerraMetrics, Map data ©2016 Google, 200 km 
ZENRIN

Figure 1: Study area with borehole locations Shenhu and Xisha [7].

Method

Test equipment

Figure 2 shows a schematic of the PCATS Triaxial testing apparatus used to carry out the soil analyses. A detailed description of PCATS Triaxial including the testing procedures can be found in [6]. Key features of PCATS Triaxial include an electronically controlled pressure volume controller to direct fluid at accurate and precisely controllable flow rates through a sample for permeability determinations, a resonant column to determine small strain shear moduli and S-wave velocities and motor drives capable of delivering axial stresses up to the mechanical failure of samples. The pressures of different system sections can be addressed and monitored independently to establish desired confining pressures and measure hydraulic gradients across a test specimen.

Sample selection and transfer into PCATS Triaxial

Pressurised sediment cores recovered from the seabed in Geotek Coring's Pressure Corer with Ball valve (PCTB) autoclave coring tool were transferred into the Geotek Pressure Core Analysis and Transfer System (PCATS) at in-situ hydrostatic pressures. The PCTB cores were contained in PVC (polyvinyl chloride) liners of 53 mm inner diameter and had a maximum length of 3.5 – 4.0 m. PCATS allowed the non-destructive characterisation of the pressurised cores based on X-Ray images, γ -density (ρ_γ) and P-wave velocity (V_p) data, as well as the cutting of subsamples for further analysis elsewhere. Subsamples selected for further analysis were transferred at pressure into storage or transfer chambers flanged to PCATS. The subsections chosen for testing in PCATS Triaxial were cut to approximately 11 cm length and transferred into the Triaxial Transfer Vessel (TTV). A summary of samples selected for triaxial testing is given in Table 1.

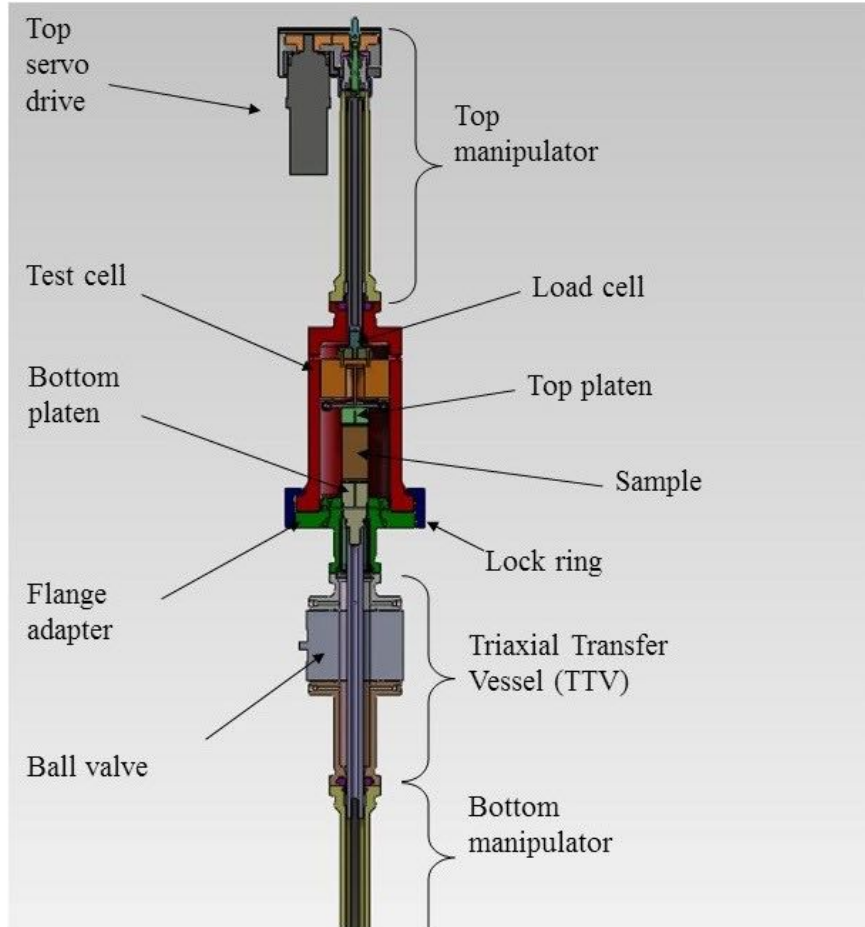


Figure 2: Schematic of PCATS Triaxial

GMGS4 Sample ID	Section depth [cm]	Sub-bottom depth [mbsf]	Water depth [mbsl]	In-situ effective stress [kPa]	$V_p^{*)}$ [m/s]	$\rho_r^{*)}$ [kg/m ³]
SC-W01B-8A-8	259-270	137.59	1287	700	1575	1700
SC-W01B-14A-6	70-81	155.70	1287	730	1693	1650
SC-W01B-15A-5	191-202	159.91	1287	760	2154	1571
SC-W01C-5A-7	156-167	148.56	1287	715	2394	1728
SC-W02B-15A-4	96-107	149.96	1272	770	2193	1720
SH-W07B-14A-2	70-81	137.60	914	760	1815	1670
SH-W07B-16A-4	109-120	144.09	914	800	1925	1640
XH-W03B-09A-3	113-124	96.13	1777	700	1479	1500
XH-W06B-07A-3	117-128	69.17	1923	600	1545	1706

Table 1: Sampling depths and properties determined with the Geotek Pressure Core Analysis and Transfer System (PCATS). In-situ effective stresses were calculated based on LWD neutron porosities, standard mineral and seawater densities and thicknesses of the overburden. *) Data from PCATS.

Within the TTV, the liner containing the sample was housed in a 65 mm ID chamber between the bottom platen sealing the bottom end of the TTV and a closed ball valve at the top. After connecting the TTV to the Bottom Manipulator via a threaded connection in the bottom platen, the assembly was mounted vertically into the frame of

the PCATS Triaxial testing apparatus. The ball valve on top of the assembly was then flanged to the triaxial test cell via flange adapter. The test cell contained the top platen and the resonant column. The top platen is linked to a load cell. Two sight windows in the test cell allowed visual inspection of the sample during testing. The test cell and top manipulator represented a closed system as these sections were pressurised with air whereas all other sections in PCATS Triaxial, including the sample, were under hydraulic pressure. Both top and bottom platens could be moved up and down by motor driven bottom and top manipulators.

A total of nine sections were subsampled from pressurised cores obtained with the PCTB coring tool. The cores were recovered from six different sites (Table 1), four of which were located in the Shenhui study area (sites SC-W01B, SC-W01C, SC-W02B, SH-W07B) and two in the Xisha study area (sites XH-W03B, XH-W06B).

Sample extrusion

To transfer the sample into the test cell the pressure was equilibrated throughout the system. Once equilibrated the ball valve inside the TTV was opened to allow upward transfer of the sample toward the test cell via actuation of the bottom manipulator. During the upward motion the sample was extruded from its liner within the flange adapter between the TTV and the test cell. Upward motion was maintained until contact of the sample with the lowered top platen was registered by the load cell. After this Bottom and Top Manipulator were synchronously driven upward to extrude the sample into a membrane in the test cell. During the extrusion the 0.5 mm thick butylene membrane unrolled over the sample, effectively sealing the latter off against the confining gas atmosphere of the test cell. The process was visually inspected through the sight windows in the test cell. Once fully extruded exact sample heights were recorded.

Sample consolidation

Consolidation followed by stepwise application of effective stresses up to the calculated in-situ values (Table 1). Consolidation after each step was considered complete after volumetric fluid release rates from the sample were considered constant over the period of time predicted for subsequent permeability measurements.

Small strain testing

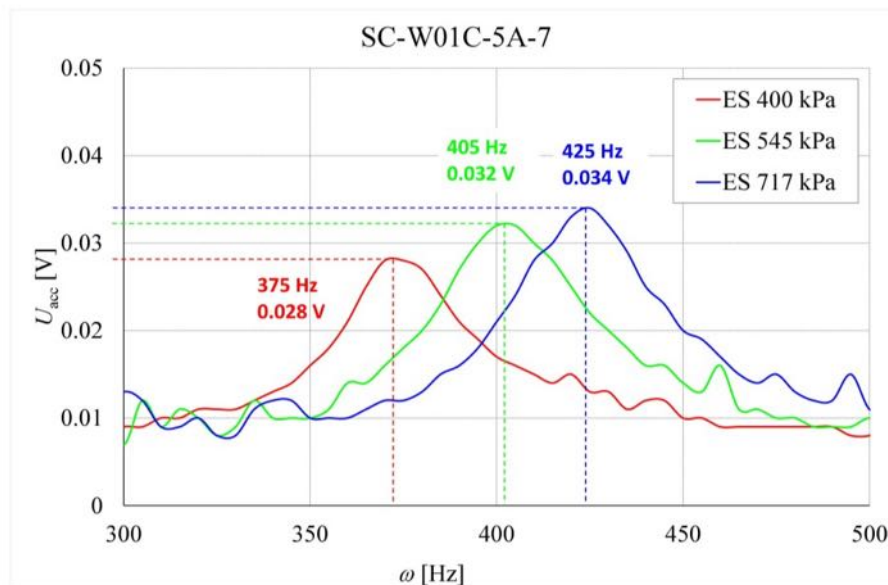


Figure 3: Example of accelerometer output vs induced frequency of torsional vibration during sample consolidation. Resonance frequencies increase with degree of consolidation as effective stress rises up to in-situ values.

After each consolidation step a resonant column test was performed. A torsional vibration was applied to the sample by oscillating the top platen. An accelerometer was used to convert amplitudes of oscillating frequencies to voltages.

The induced oscillating frequencies were incrementally increased and resulting output voltages recorded. Resonance was readily discernible by increased output voltages such as shown as example in Figure 3. Employing the theory of vibration of a linearly visco-elastic cylindrical rod, resonance frequencies were used to calculate shear wave velocities V_s and from these small strain shear moduli, G_{max} . Resonant column tests were run after each consolidation step, yielding up to three data sets for each sample. Due to initial malfunctioning of the resonant column no data could be obtained for samples SC-W01B-8A-8 and SC-W01B-14A-6.

Permeability testing

Once samples were consolidated at final in-situ effective stresses, permeability measurements were commenced. Using the pressure volume controller, fluids were directed upward and downward through the samples at constant flow rates. Pore pressures at the top and bottom of the sample were monitored and vertical permeabilities determined from Darcy's law once the hydraulic gradient reached constant values. A capillary with a known permeability was used to identify instrumental artefacts introduced into the measurements. Efforts were made to perform at least two permeability measurements for each sample with fluid directed at a volumetric flow rate $Q = 100$ nL/s, both upward and downward through the sample. However, due to the tight work schedule offshore this could only be achieved for sample SC-W01B-8A-8. All other permeabilities were determined from only one measurement. Measurements of samples SC-W01B-15A-5 and SC-W02B-15A-4 were conducted at 200 nL/s.

Figure 4 shows developments of hydraulic gradients for samples where pore fluid was directed upward through the samples at a rate Q of -100 nL/s. Since $\Delta P_{pore} = P_{pore, top} - P_{pore, bottom}$, upward flow eventually resulted in negative values, from which permeabilities were calculated. The initial increase of ΔP_{pore} is attributed to pore water loss due to ongoing consolidation at the time the measurements commenced. Minute drops in gas pressure in the test cell resulted in slight loss of confining pressure during testing. Repressurisation to compensate for this loss lead to the marked positive jumps in ΔP_{pore} , most conspicuously at 4.7 h into testing SH-W07B-16A-4. Sample SC-W01C-5A-7, remoulded was not included in Figure 4, since inevitable loss of material during sample recovery and subsampling reduced its length to 73 mm (vs 104 – 110 mm for shown samples).

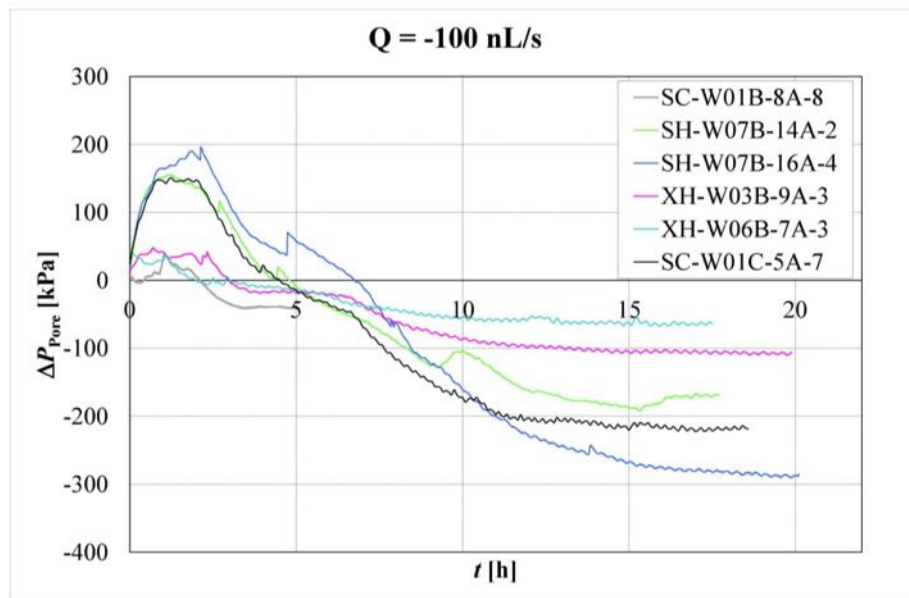


Figure 4: Development of hydraulic gradients across samples in response to setting flow to -100 nL/s (the negative sign denotes upward flow direction).

Additional permeability data were derived from in-situ cone penetration tests (CPT). The targeted locations included borehole sections in close proximity to and similar LWD characteristics as those selected for testing in PCATS Triaxial, allowing comparison of permeabilities derived via the two methods.

Large strain testing

After permeability measurements were completed, samples were subjected to undrained triaxial testing. The tests occurred at in-situ stresses except for samples SC-W01B-15A5 and SC-W02B-15A-4, which were performed at effective stresses of 2200 kPa and 1200 kPa, respectively. Axial strains were increased at rates of 1 % of the sample height per h and the resulting deviatoric stress, q , was recorded. Strain rates were maintained beyond sample failure or until the torque limit of the manipulator drive delivering the load to the samples was reached. Shear strengths were derived from peak deviatoric stresses, when samples showed strain softening, or from q at local minima of mean effective stresses, p' .

Degassing

To determine gas hydrate content, sheared samples were subjected to controlled depressurisation. During depressurisation effective stresses were maintained at positive values to avoid fluid loss from the sample into the gas filled test cell. Fluids released from the sample during depressurisation were bled via a degassing manifold connected to PCATS Triaxial and collected at 8 °C and atmospheric pressure in a water filled, inverted 2000 mL measuring cylinder. The latter was immersed in a tall cylindrical vessel filled with water to a known level. Fluids entered the measuring cylinder from beneath through a rising tube installed in the base of the cylindrical container and connected to the sample bleed point of PCATS Triaxial. Volumes of both gas and water were determined from water displacement in the inverted measuring cylinder and the rise of the water level in the cylindrical vessel, respectively. The collected gas phase was sampled and subjected to gas chromatographic (GC) analysis. The amount of gas hydrate was calculated from the total volume of the collected hydrate forming gas, based on a hydration number of 6. Results were expressed as pore volume fraction. All samples were depressurised in this fashion.

The PCATS Triaxial degassing data complements the data set obtained from an extensive quantitative degassing program targeting selected subsamples of each autoclave core successfully recovered during GMGS4. Hydrate saturations from subsamples in close proximity to those degassed in PCATS Triaxial and with similar V_p are included here for comparison and data quality control.

Grain size analysis

After complete depressurisation the triaxial test cell was opened to recover the sample. Aliquots from recovered samples were taken for grain size analyses. Analyses were performed on a Malvern 2000 Mastersizer. Due to limited analytical capacity on board grain sizes of samples SH-W07B-14A-2 and XH-W06B-7A-3 could not be determined.

Additional testing

To highlight the effect of gas hydrate content on the measured soil mechanical properties, the recovered, de-gassed sediment of Sample SC-W01C-5A-7 was remoulded and consolidated in a PCTB liner for renewed testing in PCATS Triaxial following the aforementioned procedure.

Results and Discussion

Table 2 summarises the results of testing subsamples with PCATS Triaxial.

Lithology

All samples consisted of light grey, clayey silt. Figure 5 shows the grain size distribution of samples recovered after controlled depressurization in PCATS Triaxial. The recovered sediments were light grey in colour, predominantly composed of grains of the silt fraction with admixtures of clay (12 – 15%) and a coarser than silt fraction (0 - 20%).

Gas hydrate saturation, S_H

Gas hydrate saturations $> 5\%$ were found in samples SC-W01B-15A-5, SC-W01C-5A-7, SC-W02B-15A-4, SH-W07B-14A-2 and SH-W07B-16A-4 (Figure 6). The comparison with S_H from subsamples depressurised in degassing chambers reveals some differences although care was taken to include only those subsamples in the comparison that were adjacent or in close proximity to and showed similar V_p as the subsamples degassed in PCATS Triaxial. However, Figure 6 shows that differences in S_H exist even among similar subsamples exclusively depressurised in degassing chambers (e.g. SCW02B-15A-2/-3), indicating that the difference in S_H is more affected by small scale sample heterogeneity rather than instrumental bias. However, sample SC-W01B-15A is an exception to this finding. The GC analysis of the gas collected during depressurisation of subsample -5 in PCATS Triaxial

Sample	S_H [%]	V_s [m/s]	G_{max} [MPa]	S_U [MPa]	κ [mD]
SC-W01B-8A-8	0.7	no data	no data	0.30	0.113
SC-W01B-14A-6	4.6	no data	no data	0.24	0.0157
SC-W01B-15A-5	40*	724	948	1.10	0.0672
SC-W01C-5A-7	55	676	827	0.62	0.0305
SC-W02B-15A-4	46	541	513	1.10	0.0120
SH-W07B-14A-2	32	591	610	0.41	0.0394
SH-W07B-16A-4	33	581	595	0.45	0.0227
XH-W03B-09A-3	0	295	163	0.28	0.0458
XH-W06B-07A-3	0	378	294	0.31	0.0860
SC-W01C-5A-7 PC	0	410	268	0.38	0.0130

Table 2: Summary of PCATS Triaxial test results. *Value estimated based on S_H of adjacent subsamples; the measured S_H of 21% was proven to be erroneous (see Figure 7).

showed up to 71% air in the recovered gas, suggesting a punctured membrane allowed gas exchange between the confining air and the sample. Therefore, the derived hydrate saturation of 21% must be regarded as minimum value. This suggestion is supported by Figure 7, which illustrates the effect of gas hydrate content on V_P based on selected subsamples from core W01B-15A. Subsamples -4 and -7 have similar V_P as the PCATS Triaxial subsample -5. However, measured S_H were significantly higher (42% in subsample -4, 37% in subsample -7). On the other hand, the effect of low S_H on V_P is clearly visible in subsample -3, where in fact, the upcore decreasing velocity trend suggests a dilution of the 7% hydrate saturation measured for the bulk subsample. Based on these considerations a true S_H , similar to subsamples -4 and -7, i.e. 40%, is plausible.

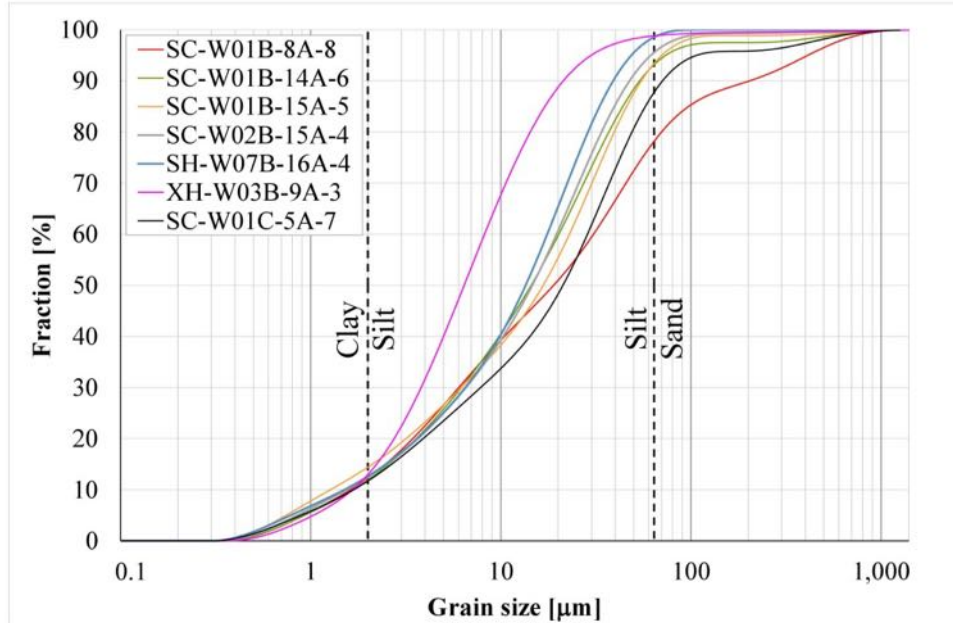


Figure 5: Grain size fractions (%). The shown samples from the Shenhu sites (SC- and SH-) exhibit a narrow grain size composition. The only Xisha site shown deviates slightly towards finer grains.

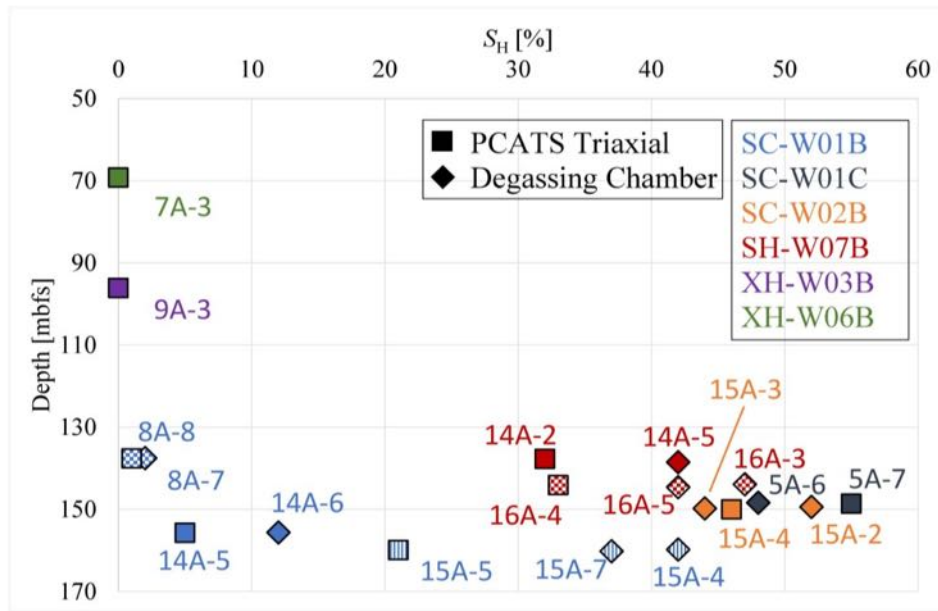


Figure 6: Pore volume gas hydrate saturations, S_H , from controlled depressurisation of subsamples. Square symbols indicate results obtained via degassing in PCATS Triaxial. Diamonds represent data from lithologically similar subsamples, degassed in pressure chambers and are included here for comparison.

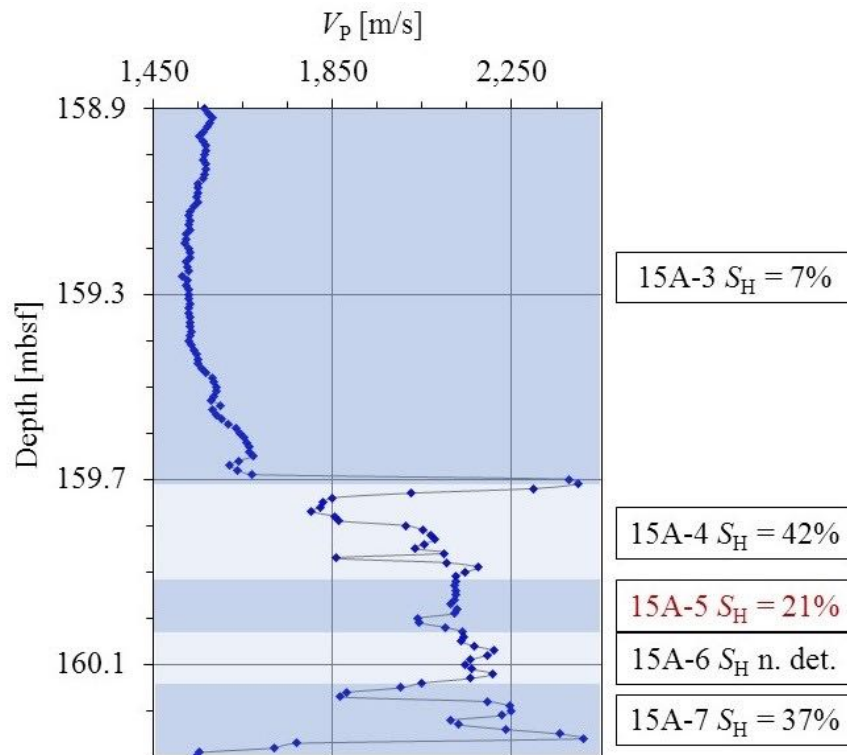


Figure 7: V_P and S_H of subsamples -3 through -7 from core SC-W01B-15A. Only subsample -5 was analysed in PCATS Triaxial. Accidental invasion of air into the collected gas during depressurisation of 15A-5 yielded an S_H lower than the actual value. Comparison with the similar subsamples -3 and -7 make a true S_H of 40% plausible. Data for subsample -6 was unavailable at time of writing.

Elastic properties (V_s and G_{small})

Shear wave velocities, V_s , and small strain shear moduli (G_{max}) derived from resonant column tests during consolidation of the samples by application of increasing effective stress are shown in Figures 8 and 9, respectively.

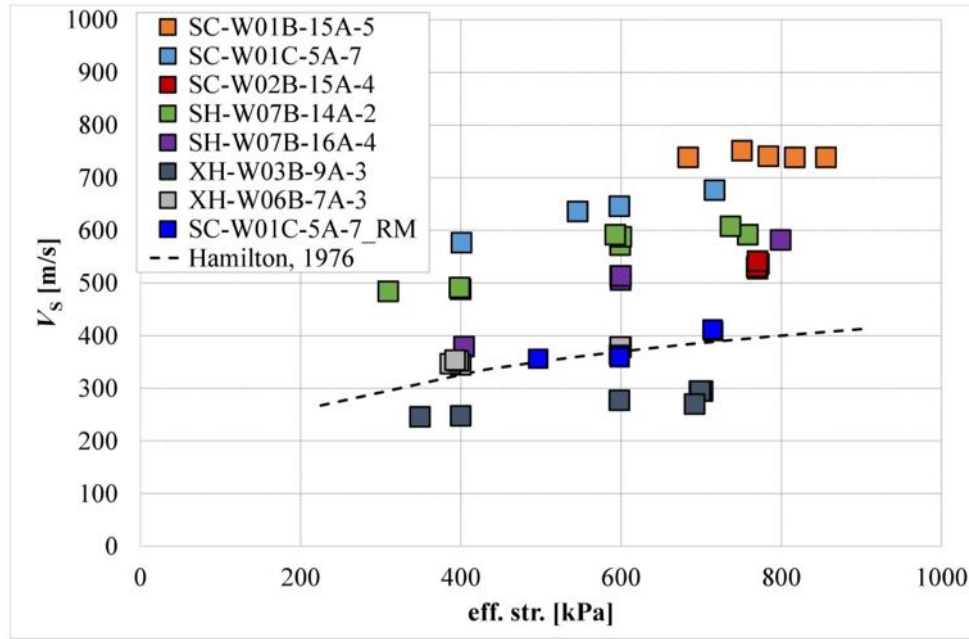


Figure 8: Shear wave velocities derived from resonance column tests during sample consolidation. SC-W01C-5A-7_RM represents remoulded sample. Shear velocities reported by Hamilton [8] for turbidites and silty clays without gas hydrates are shown for reference.

Except for sample SC-W01B-15A-5 maximum effective stresses for each sample represent the calculated in-situ values (Table 1). In these cases, V_s increased with the incrementally raised effective stress. In contrast, sample SC-W01B-15A-5 was initially consolidated at 856 kPa, exceeding the true in-situ value by 96 kPa. Although the effective stress was later reduced to the true in-situ value (760 kPa), measurements at this condition did not yield significantly different resonance frequencies. This indicated the short-term irreversibility of overconsolidation and suggests lower than measured V_s and G_{max} at true in-situ stress conditions for this sample. Based on linear fits to effective stress and V_s of the other gas hydrate bearing samples (SC-W01C-5A-7, SH-W07B-14A-2 and SH-W07B-16A-4), calculation of V_s for sample SC-W01B-15A-5 at the actual in-situ stress of 760 kPa infers a true in-situ shear wave velocity of 702 m/s.

V_s and G_{max} of gas hydrate-rich subsamples plot well above those without or with low gas hydrate contents. In turn, V_s of the latter coincide or plot below V_s reported by Hamilton [8] for (gas hydrate free) turbidites and silty clays (Figure 8). The exceptional coincidence of V_s of the remoulded and thus hydrate free sample SC-W01C-5A-7_PC with the literature data is striking and demonstrates the reliability of the measuring technique. V_s and S_H were found to be linearly well correlated (Figure 10). This finding might become an important diagnostic aid in estimating resource potential of gas hydrates in the South China Sea based on remote sensing techniques.

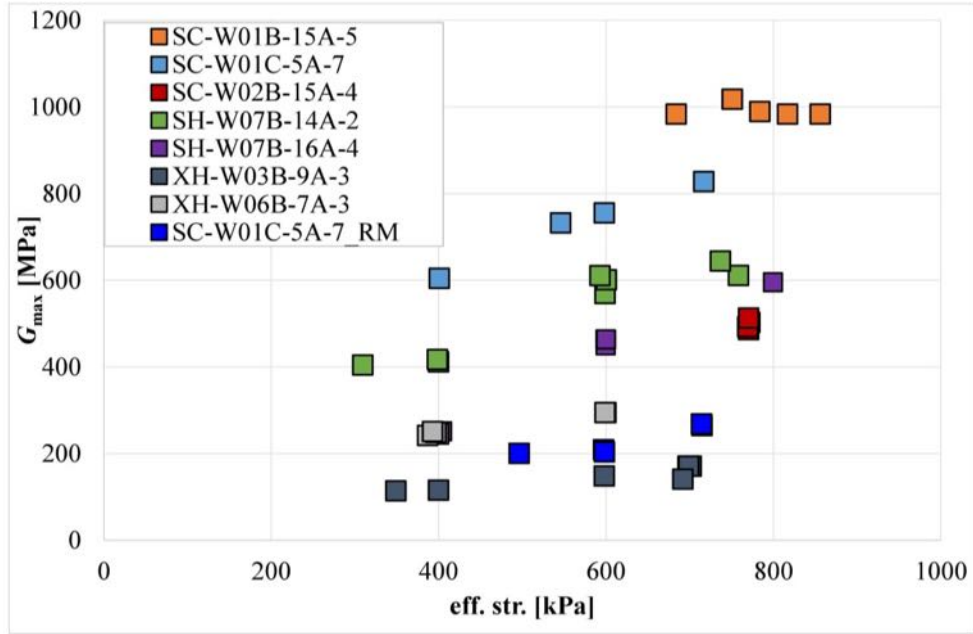


Figure 9: Small strain shear moduli derived from resonance column tests during sample consolidation. SC-W01C-5A-7_RM represents remoulded sample.

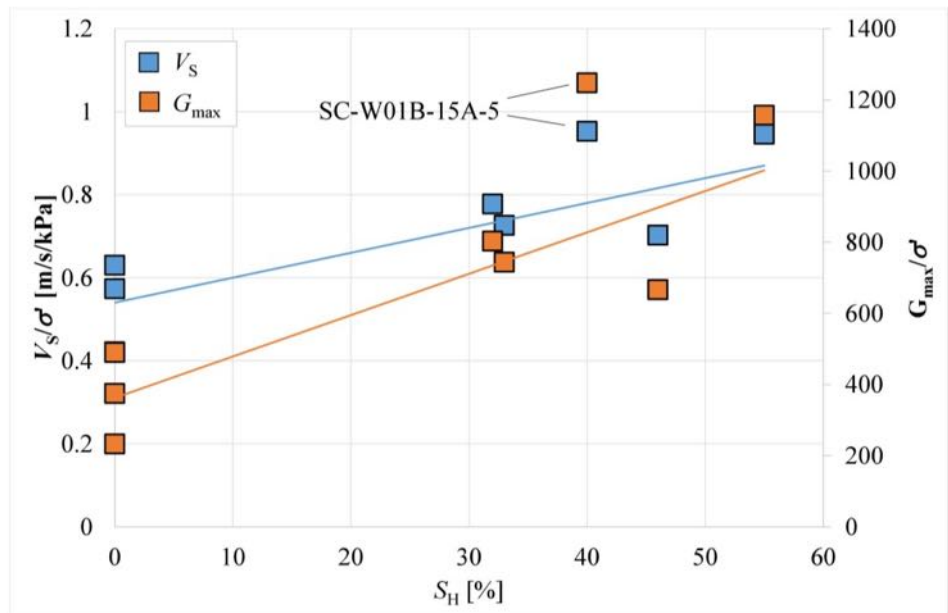


Figure 10: Effective stress-normalised V_s and G_{max} are well linearly correlated to S_H ($R^2 = 0.73$ and 0.80 , respectively). The data points for subsample SC-W01B-15A-5 were not included in the regression due to the uncertainty associated with S_H .

Shear strength, S_U

S_U range from 0.24 MPa (SC-W01B-14A-6) to 1.1 MPa (SC-W01B-15A-5 and SC-W02B-15A-4, Table 2). Four samples (SC-W01B-8A-8, SC-W01B-15A-5, SH-W07B-14A-2 and XH-W06B-7A-3) exhibited strain softening whereas all other samples displayed strain hardening behavior in response to increasing deviatoric stress. The latter typically results in barrel-type, plastic deformation as shown by sample XH-06B-7A-3 (Figure 11).



Figure 11: Samples XH-06B-7A-3 and SC-W01B-15A-5 after recovery from PCATS Triaxial. The barrel-type deformation shown by the former sample on the left is indicative of plastic deformation and strain hardening, while the clearly visible shear plane of the latter (right) indicates sudden failure typical to a brittle soil. The vesicles in the image on the right indicate ongoing degassing after recovery of SC-W01B-15A-5.

In accordance to the elastic data (V_s , G_{max}), S_U of hydrate bearing subsamples exceed those without hydrate. The observation that gas hydrates promote the shear strength of similar fine grained sediments from the South China Sea has recently been demonstrated qualitatively in laboratory tests by Luo and coworkers [9], who enriched natural marine sediments and commercially available aggregates matching the grain sizes of this study with synthesised gas hydrates. This study furthermore reveals a linear correlation between the effective stress-normalised shear strength and S_H ($R^2 = 0.73$, Figure 12). This finding is in good agreement with the correlation of effective stress-normalised V_s and S_H presented in Figure 10.

Permeability, κ

Permeabilities calculated from ΔP_{pore} at steady state conditions varied from 0.012 - 0.113 mD (Figure 13). CPT derived permeabilities are shown for comparison and exceed those from testing in PCATS Triaxial by two orders of magnitude. It should be noted that permeabilities in PCATS Triaxial are derived by directing the test fluid through the sample normal to the seabed. Hence, the derived permeabilities are vertical, and may deviate significantly from horizontal permeabilities in strongly anisotropic samples. On the other hand, CPT of anisotropic samples largely yields horizontal permeabilities, as the excess pore pressure building up during penetration of the cone is released via preferential pathways existing between parallel-bedded mineral grains. The effect may be amplified by gas hydrate formation, which preferentially occurs in layers if lateral fluid flow and dissolved gas transport is facilitated with respect to vertical transport. Although permeability discrepancies seem to be equally high in both hydrate-rich and hydrate-poor samples (Figure 13), it should be noted that the aforementioned effect of hydrate formation parallel to the bedding may not be easily visible in such a comparison. Since the lateral conductivity is determined by the layer with highest conductivity, while the vertical conductivity is controlled by the layer with lowest hydraulic conductivity, occasional layers of hydrate may already reduce the vertical permeability quite significantly without affecting the lateral conductivity at all. In addition to these intrinsic effects CPT may have introduced fractures to the sediment, greatly enhancing the hydraulic conductivity. While these artefacts may or may not have been

In contrast to elastic properties and shear strength, where the influence of hydrate is evident, the effect of hydrate saturation on permeability is less apparent (Figure 14). Although the hydrate-devoid sample SC-W01B-8A-8 exhibits the highest permeability, the vertical permeability is only poorly correlated to S_H ($R^2 = 0.36$).

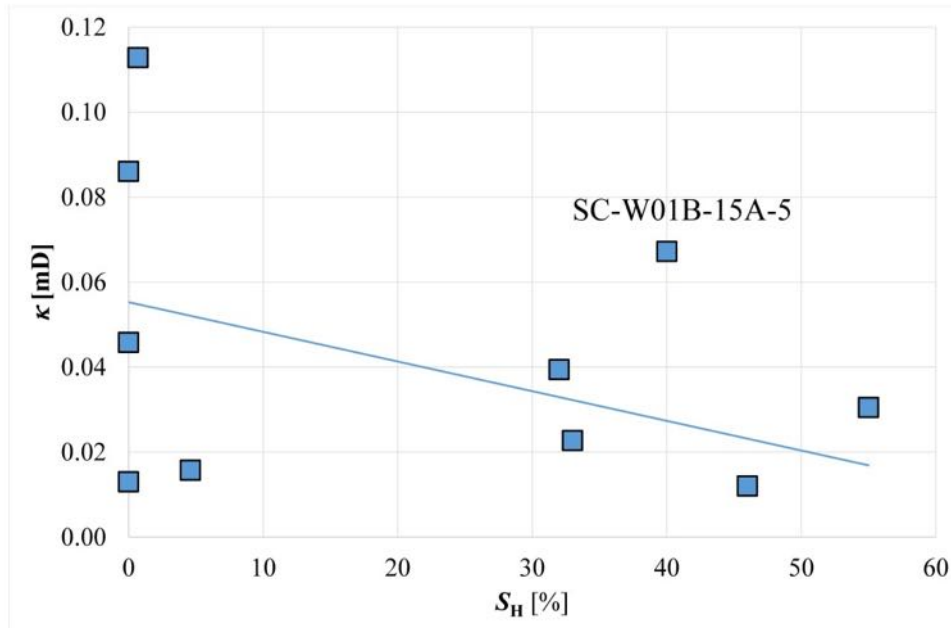


Figure 14: Vertical permeabilites vs S_H as determined in PCATS Triaxial.

Interestingly, the direct comparison of the undisturbed sample SC-W01C-5A-7 ($S_h = 55\%$) with its remoulded counterpart ($S_h = 0$) reveals a higher permeability in the hydrate bearing sample. This is in strong contrast to observations in coarser host sediments, where the permeability of a hydrate bearing sand ($S_h = 70\%$) was reduced by two orders of magnitude after the hydrate had been dissociated although not remoulded [6]. While sands exhibit a hydraulic anisotropy close to unity the above observations suggest that the hydraulic behavior of hydrate-bearing, fine grained sediments (silts and finer) are largely controlled by hydraulic anisotropy rather than bulk hydrate content.

Conclusions

Triaxial testing of pressure core segments at in-situ conditions revealed a number of important parameters relevant to gas production from fine grained gas hydrate bearing sediments in the South China Sea. A strong dependency of shear wave velocity, small strain shear modulus and shear strength on hydrate saturation could be demonstrated, affirming the importance of gas hydrates in studies of marine slope stability. The studied samples were dominated by grains of the silt fraction with minor admixtures of clay and coarser sediments. Vertical permeabilities fell below 0.12 mD and were poorly correlated with gas hydrate saturation. The vertical permeabilites differed by two orders of magnitude from permeabilites obtained via cone penetration tests indicating a strong sample anisotropy, possibly augmented by interbedded hydrate layers. A poor correlation of gas hydrate saturation and permeability in these fine grained sediments has been shown for the first time and contrasts previous observations made in coarser sediments. This finding is of great technical importance and highlights the importance of further investigations.

References

- [1] E.D. Sloan, C.A. Koh, "Clathrate Hydrates of Natural Gases", 3rd ed., CRC Press, Chemical industries series 119, 2008
- [2] P.J. Schultheiss, T.J.G Francis, M. Holland, J.A. Roberts, H. Amann, Thjunjoto, R.J. Parkes, D. Martin, M. Rothfuss, F. Tuynder, P.D. Jackson, "Pressure Coring, Logging and Sub-Sampling with the HYACINTH

- system”, *Sediment Core Analysis*, Geol. Soc. London, 2006. Spec. Pub. 267. pp. 151–163.
- [3] P.J. Schultheiss, M. Holland, J.A. Roberts, Q. Huggett, M. Druce, P. Fox, “PCATS: Pressure Core Analysis and Transfer System” Proc. 7th Intl. Conf. Gas Hydrates (ICGH 2011), Edinburgh, UK, 17-21 July 2011
- [4] P.J. Schultheiss, J.A. Roberts, M. Druce, J. Priest, M. Holland, K. Yamamoto, S. Yang, “PCATS and PCATS Triaxial: further development and recent field experience making core measurements under pressure” Proc. 8th Intl. Conf. Gas Hydrates (ICGH 2014), Beijing, China, July 29-Aug 2 2014
- [5] T.S. Yun, G.A. Narsilio, J.C. Santamarina, C. Ruppel, “Instrumented pressure testing chamber for characterizing sediment cores recovered at in-situ hydrostatic pressure”, *Marine Geology*, 229 (3-4), 285-293, 2006
- [6] J.A. Priest, M. Druce, J. Roberts, P. Schultheiss, Y. Nakatsuka, K. Suzuki, “PCATS Triaxial: A new geotechnical apparatus for characterizing pressure cores from the Nankai Trough, Japan”, *Marine and Petroleum Geology*, <http://dx.doi.org/10.1016/j.marpetgeo.2014.12.005>, 2015
- [7] South China Sea. (14.09.2016). Google Maps. Google. Retrieved from <https://www.google.co.uk/maps/@17.3598535,114.8666787,2096433m/data=!3m1!1e3>.
- [8] E. Hamilton, “Shear-wave velocity versus depth in marine sediments: a review”, *Geophysics* 41: 985–996, 1976
- [9] T. Luo, Y. Song, Y. Zhu, W. Liu, Y. Liu, Y. Li, Z. Wu, “Triaxial experiments on the mechanical properties of hydrate-bearing marine sediments of South China Sea”, *Marine and Petroleum Geology* 77: 507-514, 2016